



CHALMERS
UNIVERSITY OF TECHNOLOGY

Field-Free Spin-Orbit Torque Switching of Canted van der Waals Magnets

Downloaded from: <https://research.chalmers.se>, 2025-05-12 02:51 UTC

Citation for the original published paper (version of record):

Zhao, B., Pandey, L., Ali, K. et al (2025). Field-Free Spin-Orbit Torque Switching of Canted van der Waals Magnets. *ACS Nano*, 19(14): 13817-13824. <http://dx.doi.org/10.1021/acsnano.4c16826>

N.B. When citing this work, cite the original published paper.

Field-Free Spin–Orbit Torque Switching of Canted van der Waals Magnets

Bing Zhao,* Lalit Pandey, Khadiza Ali, Erdi Wang, Craig M. Polley, Balasubramanian Thiagarajan, Peter Makk, Marcos H. D. Guimarães, and Saroj Prasad Dash*



Cite This: *ACS Nano* 2025, 19, 13817–13824



Read Online

ACCESS |

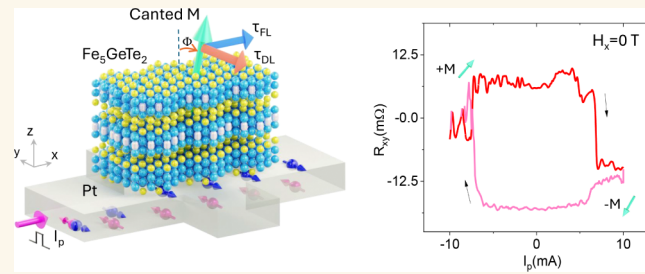
Metrics & More

Article Recommendations

Supporting Information

ABSTRACT: Spin–orbit torque (SOT) magnetization switching is crucial for next-generation energy-efficient spintronic technologies. The recent discovery of van der Waals (vdW) magnets holds promise for such SOT phenomena because of their tunable magnetic properties. However, a demonstration of energy-efficient and field-free SOT switching of vdW magnets is required for their potential applications. Here, we demonstrate field-free and deterministic switching using an intrinsic canted vdW magnet Fe_5GeTe_2 in a heterostructure with Pt having a larger spin Hall conductivity up to room temperature. Using anomalous Hall electrical detection for magnetization readout, we reveal that field-free deterministic SOT switching in the $\text{Fe}_5\text{GeTe}_2/\text{Pt}$ Hall devices can be attributed to the canted magnetic anisotropy of Fe_5GeTe_2 , originating from its crystal and magnetic structures. Detailed second harmonic Hall measurements exhibit a high spin Hall conductivity $\sigma_{\text{SH}} \sim 3 \times 10^5 \text{ h}/2e \Omega^{-1} \text{ m}^{-1}$ with an SOT effective damping-like field of 0.06 mT per MA/cm². These findings reveal efficient and field-free SOT phenomena in the canted vdW magnet Fe_5GeTe_2 up to room temperature and highlight their usefulness in spintronic devices.

KEYWORDS: canted magnetization, spin–orbit torque, Fe_5GeTe_2 , 2D magnets, 2D materials, room temperature



INTRODUCTION

Energy-efficient spintronic technologies are expected to provide solutions for next-generation nonvolatile computing architectures.^{1,2} After the successful utilization of giant magnetoresistance (GMR) and tunnel magnetoresistance (TMR) in data storage and spin-transfer-torque (STT) based nonvolatile memory technologies,³ an energy-efficient spin–orbit torque (SOT) phenomenon is considered for faster and ultralow power switching of a nanomagnet for memory,^{4–6} logic,⁷ and neuromorphic computing.^{8,9} In a heterostructure of high spin–orbit material and a ferromagnet, a charge current flowing through the spin–orbit material generates a spin current, which exerts SOT to switch the magnetization of the ferromagnet. However, the requirement of high drive current, the needed assistance of an external magnetic field, and the lack of external control for deterministic SOT switching are the fundamental obstacles to technological applications.^{10,11}

Recently discovered van der Waals (vdW) magnets are crucial for SOT technology owing to their low dimensionality, tunable magnetic anisotropy with composition and temperature, proximity-induced phenomena, as well as the possibility of voltage-controlled magnetism.^{12–15} This opens enormous prospects for resolving the material challenges of using traditional ultrathin ferromagnetic metal films^{6,16} and artificial heterostructures.^{17–20} Energy-efficient SOT was demonstrated

using vdW magnets with perpendicular magnetic anisotropy (PMA) such as Fe_3GeTe_2 ,^{21,22} Fe_3GaTe_2 ,^{23,24} and $\text{Cr}_2\text{Ge}_2\text{Te}_6$ ²⁵ in heterostructure with conventional heavy metal Pt^{21,22} or topological insulators (TIs).^{26,27} However, the SOT devices of vdW magnets with strong PMA in heterostructure with Pt or TIs provide an in-plane current-induced spin polarization and need an external in-plane magnetic field to break the symmetry for deterministic magnetization switching.¹⁶ Recently, field-free deterministic SOT switching of vdW magnets with PMA (Fe_3GeTe_2 and Fe_3GaTe_2) has been demonstrated in heterostructures with WTe_2 and TaIrTe_4 using their out-of-plane SOT component.^{28–34} However, this requires a higher current density for magnetization switching as the spin Hall conductivities of WTe_2 ^{35,36} and TaIrTe_4 ^{32,33} are limited to $\sigma_{s,z} \sim 10^3–10^4 \text{ h}/2e\Omega^{-1}\text{m}^{-1}$, which is orders of magnitude lower than Pt with $\sigma_{s,y} \sim 10^5 \text{ h}/2e\Omega^{-1}\text{m}^{-1}$.^{21,22,37} Therefore, practical SOT tech-

Received: November 22, 2024

Revised: March 12, 2025

Accepted: March 13, 2025

Published: March 31, 2025



nologies require energy-efficient and field-free deterministic magnetization switching of vdW magnets in a heterostructure with spin-orbit materials having a larger spin Hall conductivity.

Here, we demonstrate field-free deterministic magnetization switching of an intrinsic canted vdW magnet Fe_5GeTe_2 in a heterostructure with Pt having a larger in-plane spin Hall conductivity. Using the anomalous Hall effect (AHE) electrical readout to detect the magnetization change, we demonstrate current-induced magnetization switching up to room temperature without the need for an external magnetic field. Such observed field-free SOT switching is attributed to the canted magnetic anisotropy originating from the crystal and magnetic structure of Fe_5GeTe_2 .³⁸ Furthermore, second harmonic Hall measurements and analysis show a large spin Hall conductivity $\sigma_{\text{SH}} \sim 3 \times 10^5 \frac{\hbar}{2e} \Omega^{-1} \text{ m}^{-1}$ and pulse current induced magnetization switching experiments exhibit the low power consumption $P \sim 10^{16} \text{ W/m}^3$ for the field-free SOT switching.

RESULTS

Canted Magnetization of Fe_5GeTe_2 . Fe_5GeTe_2 has gathered increasing attention because of the manifestation of magnetic order above room temperature with $T_c > 300 \text{ K}$ and its canted magnetization.^{38–41} Specifically, the canted magnetic properties are established in Fe_5GeTe_2 /graphene spin-valve devices using Hanle spin precession measurements to probe

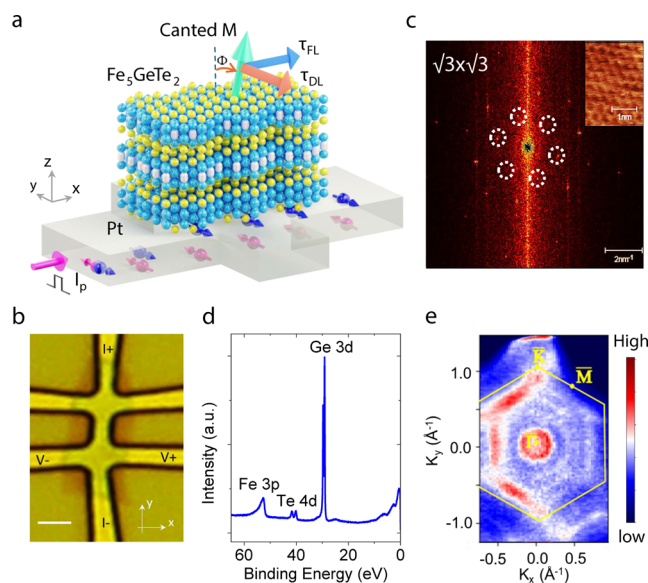


Figure 1. Spin-orbit torque device of Fe_5GeTe_2 /Pt heterostructure and characterization of Fe_5GeTe_2 . (a) Schematic of the Fe_5GeTe_2 /Pt heterostructure Hall-bar device for observation of SOT-induced magnetization switching. The pulsed charge current I_p applied to Pt generates a spin current J_s due to the spin Hall effect inducing a damping-like torque (τ_{DL}) and field-like torque (τ_{FL}) exerted on the magnetic moment M of Fe_5GeTe_2 . (b) Optical microscope image and measurement geometry of the Fe_5GeTe_2 /Pt Hall-bar device used for AHE and SOT experiments. (c) Fast Fourier transform (FFT) image of the STM topography of Fe_5GeTe_2 (inset showing the higher resolution STM image) measured at room temperature mapping with 1 V and 200 pA. (d) XPS of the Fe_5GeTe_2 shows sharp peaks of Fe, Te, and Ge, respectively, probed at 160 eV at 260 K. (e) ARPES density mapping at the Fermi surface as a function of K_x and K_y in the Fe_5GeTe_2 system taken at 20 K with photon energy 138 eV.

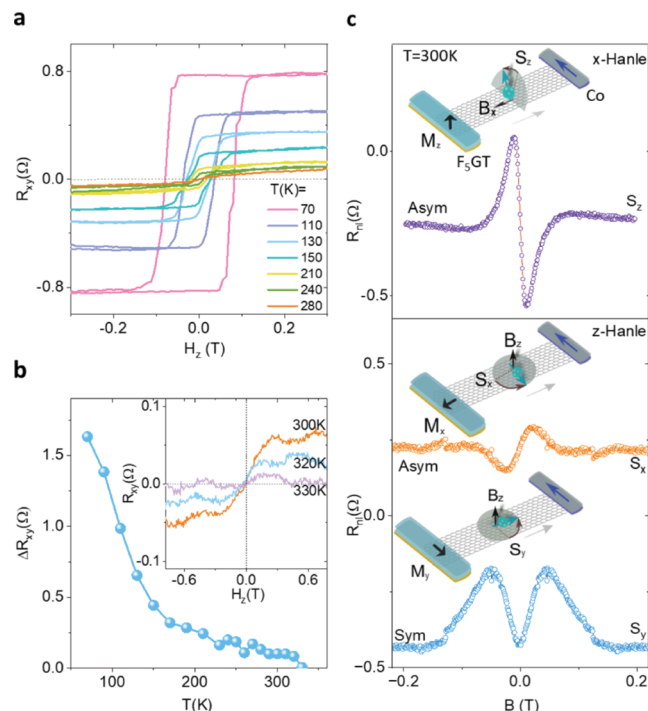


Figure 2. Magnetic properties of Fe_5GeTe_2 nanolayers with canted magnetization. (a) AHE resistance R_{xy} as a function of the perpendicular magnetic field H_z at different temperatures for a representative Fe_5GeTe_2 /Pt Hall device. (b) The temperature dependence of the AHE magnitude ΔR_{xy} . The inset shows the AHE curves above room temperature. (c) Spin injection experiments with Fe_5GeTe_2 /graphene spin-valve device. The canted magnetization of Fe_5GeTe_2 nanoflake at room temperature results in the observation of x-Hanle and z-Hanle spin precession signals with the asymmetric (Asym) and symmetric (Sym) components. The insets are the schematics for the corresponding measurements and the spin precession dynamics.

different spin components.³⁸ Such a canted magnetization in Fe_5GeTe_2 can provide a possible field-free SOT-induced magnetization switching phenomenon using a larger in-plane spin Hall conductivity of Pt. The schematic and microscope picture of the Fe_5GeTe_2 /Pt Hall-bar device used for SOT experiments are shown in Figure 1a,b (see more details on the device fabrication in Methods, Figure S1 and Table S1). In a SOT experiment, the application of a series of DC pulse currents I_p along the x-direction through the spin-orbit material (Pt), generates an orthogonal spin current J_s with spin polarization s_y along the y-axis due to the spin Hall effect. The generated spin current in Pt exerts SOTs (field-like τ_{FL} and damping-like τ_{DL} torques) to switch the magnetization of Fe_5GeTe_2 . Specifically, a field-like torque, $\tau_{FL} \sim M \times s$, precesses M about the exchange field created by spin polarization,^{42,43} while a damping-like torque $\tau_{DL} \sim M \times (M \times s)$ rotates magnetic moment M toward the direction of spin polarization.

To evaluate the quality of the Fe_5GeTe_2 crystal, we conducted a scanning tunneling microscopy (STM) analysis of bulk crystal after cleaving the surface in ultrahigh vacuum (Figure 1c). This imaging technique allowed us to resolve the crystal's atomic arrangement, verifying a $\sqrt{3} \times \sqrt{3}$ atomic structure.³⁸ We carried out an X-ray photoelectron spectroscopy (XPS) measurement (Figure 1d) to examine the elemental compositions. The XPS data confirmed the presence

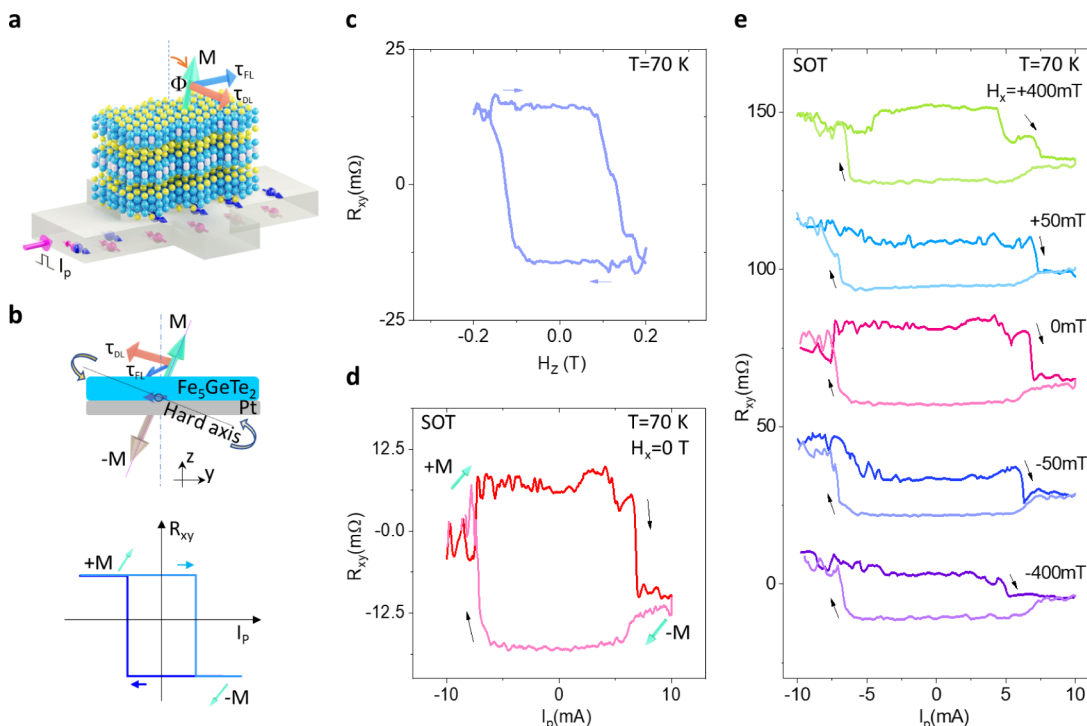


Figure 3. Field-free deterministic SOT magnetization switching of Fe_5GeTe_2 with canted magnetization. (a) Schematic of the $\text{Fe}_5\text{GeTe}_2/\text{Pt}$ heterostructure with canted magnetic (M) configuration and SOT components (field-like τ_{FL} and damping-like τ_{DL} torques). (b) Possible damping-like and filed-like SOT components with the canted magnetization anisotropy of Fe_5GeTe_2 and the expected SOT switching behavior. (c) The AHE signal measured in $\text{Fe}_5\text{GeTe}_2/\text{Pt}$ heterostructure in Dev 1 at 70 K. (d) SOT-induced magnetization switching without any external magnetic field H_x , measured with pulse current I_p with a duration of 200 μs and reads current I_r of 50 μA . (e) SOT-induced magnetization switching for different external in-plane magnetic fields $\pm H_x$.

of Fe, Ge, and Te, with no indication of doping from foreign elements or contamination by impurities. Furthermore, Figure 1e presents the Fermi surface map using angle-resolved photoelectron spectroscopy (ARPES), showing distinct band features that reveal a 6-fold symmetry corresponding to the hexagonal Brillouin zone. This observation further supports the high structural quality of the Fe_5GeTe_2 crystals.³⁸

To probe the magnetic properties of the Fe_5GeTe_2 nanolayer flake, anomalous Hall effect (AHE) measurements were carried out. The transverse magnetoresistance $R_{xy} = V_{xy}/I_{dc}$ is probed as a function of the out-of-plane magnetic field H_z . The presence of long-range magnetic order in Fe_5GeTe_2 makes it possible to observe the AHE signal, i.e., R_{xy} is proportional to the component magnetization M_z . Temperature dependence of the AHE signal (Figure 2a,b) shows a decrease in both the magnitude (ΔR_{xy}) and the coercive field (H_c) at higher temperatures. The AHE hysteresis loops measured at low temperatures show a clear magnetic remanence in Fe_5GeTe_2 . At higher temperatures, the remanence disappears, and the hysteresis loop vanishes; nevertheless, the nonlinearity of the AHE signal persists above room temperature up to 330 K.

To prove the canted magnetism of Fe_5GeTe_2 , we adopted the spin injection/detection method in $\text{Fe}_5\text{GeTe}_2/\text{graphene}$ nonlocal spin valve device.³¹ By performing the x-Hanle and z-Hanle measurements with magnetic field sweeps along x and z directions (Figure 2c), we observed that the x-Hanle signal shows only the asymmetric component and the z-Hanle signal shows both the asymmetric and symmetric components. These observations suggest the coexistence of different spin components (S_x , S_y , and S_z) and canted magnetism with $\Phi =$

$13.3^\circ \pm 0.5^\circ$ of the Fe_5GeTe_2 nanoflake at room temperature (see detailed analysis in Note S1, Figures S2 and S3).³⁸

Field-Free Deterministic Spin–Orbit Torque Magnetization Switching in $\text{Fe}_5\text{GeTe}_2/\text{Pt}$ Heterostructure. Traditionally, for a strictly perpendicular magnetization, the τ_{DL} only pulls M to the in-plane orientation, and the final magnetization state after the removal of the current can have a random magnetization unless an external field H_x is applied to generate an additional field torque allowing for deterministic switching.¹⁶ However, for a canted magnetization orientation (Figure 3a), the final magnetic state can still be deterministic (from $\pm M$ to $\mp M$) without an external field due to the geometrical symmetry breaking (Figure 3b).¹⁷

First, we present SOT-induced magnetization switching of nanolayer $\text{Fe}_5\text{GeTe}_2/\text{Pt}$ heterostructure measured at 70 K (Device schematics in Figure 3a). Figure 3c shows the AHE signal of the $\text{Fe}_5\text{GeTe}_2/\text{Pt}$ heterostructure Hall-bar device (Dev 1) with H_z sweep at 70 K. For the SOT-induced magnetization switching experiments, the Hall resistance $R_{xy} = V_{xy}/I_r$ was recorded after each pulse current I_p applied with a dwell time of 200 μs , where I_r is the reading current (50 μA). To be noted, in comparison to only Fe_5GeTe_2 measured before, in the $\text{Fe}_5\text{GeTe}_2/\text{Pt}$ bilayer devices, the AHE signal is smaller because the contacts are made on Pt and a partial current flow through Fe_5GeTe_2 . The hysteretic AHE signals with the pulse current swept between ± 10 mA (Figure 3d) are observed without the application of any magnetic field ($H = 0$), which corresponds to a critical switching current density J_{sw} of $3.2 \times 10^7 \text{ A/cm}^2$. The magnitude of the AHE loops as a function of bias current and magnetic fields are comparable, suggesting a complete switching of the magnetic moment.

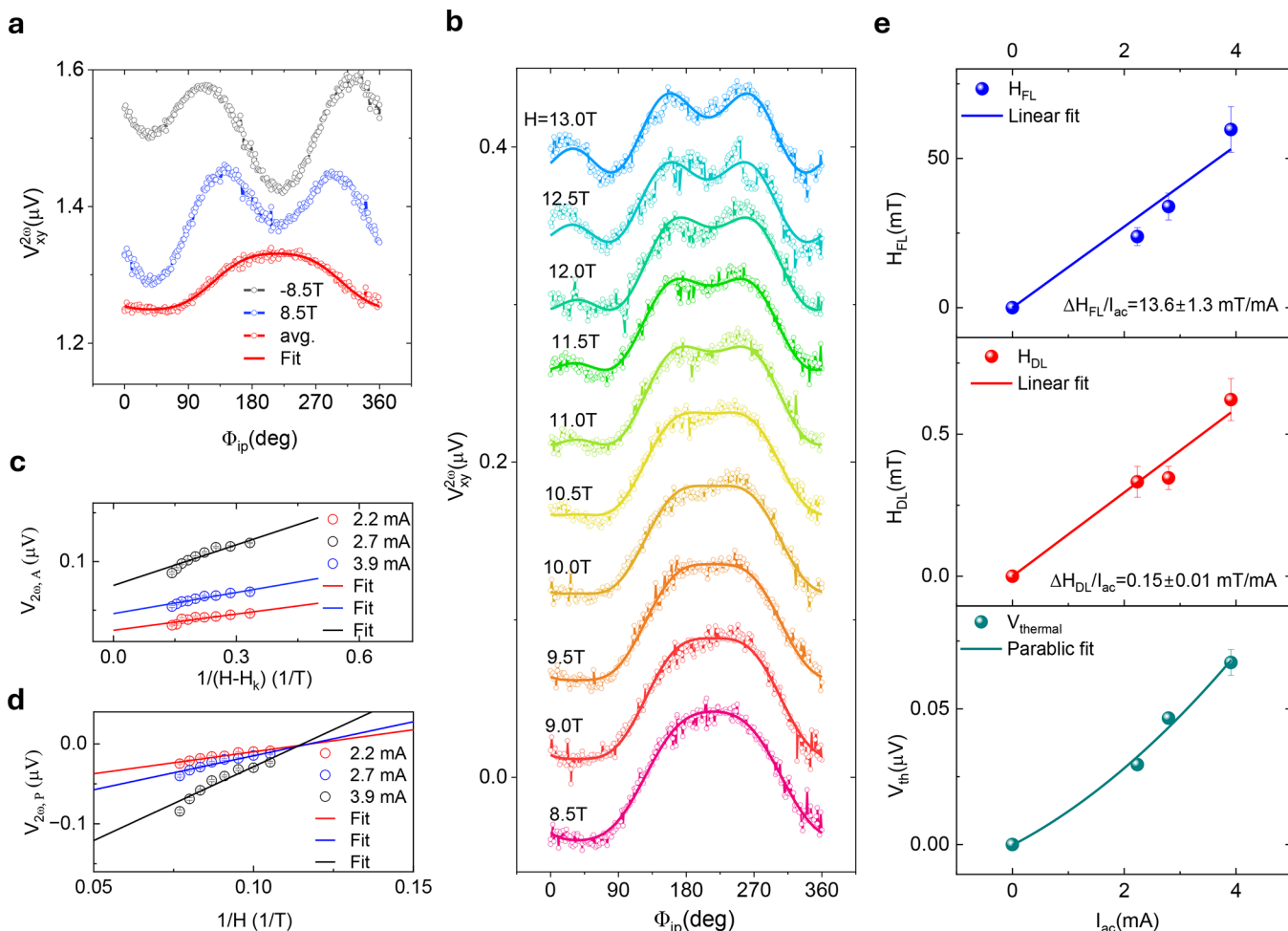


Figure 4. Second harmonic Hall measurements of the SOT effective fields in $\text{Fe}_5\text{GeTe}_2/\text{Pt}$ heterostructure. (a) In-plane angle dependence of the 2nd harmonic signals at $H = \pm 8.5$ T and the averaged signal (avg.) for $\pm H$ in Dev 2 at 120 K. The solid curve is the fitting result with eq 1. (b) Averaged second harmonic signals as a function of the in-plane angle Φ_{ip} at different external fields H . The solid curves are the fitting results with eq 1. (c,d) Extracted components $V_{2\omega,\text{A}}$ and $V_{2\omega,\text{P}}$ with different bias currents as a function of the $1/H$ and $1/(H - H_k)$, respectively. The linear solid curves are the fitting results with eqs 2 and 3. (e) Applied bias dependence of the extracted field-like (H_{FL}), damping-like (H_{DL}) and thermal contribution (V_{th}) components.

Such deterministic field-free SOT-induced magnetization switching in $\text{Fe}_5\text{GeTe}_2/\text{Pt}$ heterostructure devices can be explained by its canted perpendicular magnetization of Fe_5GeTe_2 , where the magnetic hard axis is tilted away from the sample plane. A large pulse current-induced damping-like torque τ_{DL} is needed to overcome the hard magnetization axis and switch to the other direction deterministically. To be noted, the switching direction (chirality) is determined by the canted direction of magnetization and a pulse current sweep would make it possible to switch the magnetic moment between $\pm M$, that is, the readout AHE signal R_{xy} ($\propto M_z$) shows a bistable state vs I_p (Figure 3b). Interestingly, the in-plane external field (H_x) dependence measurements show that the sign of the SOT switching direction remains unchanged (Figure 3e), suggesting that the applied field does not play a major role in the symmetry breaking for the deterministic switching. Conventionally, the SOT chirality is determined by the external field for a perpendicular magnet, which favors the opposite switching directions with the positive and negative in-plane magnetic fields.¹⁶ However, in the canted magnetic moment scenario, the in-plane spin $\pm s$, induced damping-like

torque solely determines the switching from $+M$ to $-M$ and vice versa without an external field.

2nd Harmonic Hall Spin–Orbit Torque Measurements in $\text{Fe}_5\text{GeTe}_2/\text{Pt}$ Heterostructure. To quantify the SOT effective damping-like field H_{DL} , field-like field H_{FL} , and the SOT efficiency quantified by the spin Hall conductivity σ_{SH} , we performed the harmonic Hall measurements. The second harmonic Hall signal $V_{xy}^{2\omega}$ as a function of the in-plane rotation angle Φ_{ip} can be expressed,^{44–46}

$$V_{xy}^{2\omega} = -V_{2\omega,\text{A}} \cos \Phi_{\text{ip}} + 2V_{2\omega,\text{P}}(2\cos^3 \Phi_{\text{ip}} - \cos \Phi_{\text{ip}}) \quad (1)$$

where

$$V_{2\omega,\text{A}} = V_A H_{\text{DL}} / (H - H_k) + V_{\text{th}} \quad (2)$$

and

$$V_{2\omega,\text{P}} = V_p H_{\text{FL}} / H \quad (3)$$

with AHE signal V_A , the effective perpendicular magnetic anisotropy field H_k , thermal contribution V_{th} , and planar Hall effect (PHE) signal V_p (see details in Figure S4). Figure 4a shows the measured raw data of the in-plane dependence of

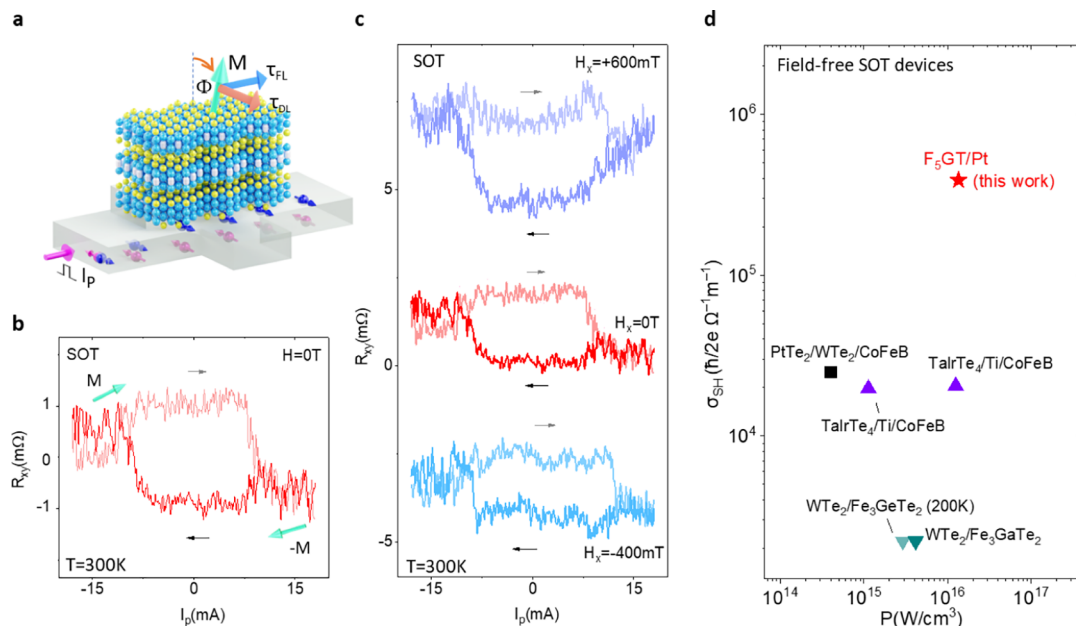


Figure 5. Room temperature field-free deterministic SOT-induced magnetization switching of Fe_5GeTe_2 . (a) Schematic of the $\text{Fe}_5\text{GeTe}_2/\text{Pt}$ SOT device with canted magnetic moment M of Fe_5GeTe_2 . (b) The SOT-induced magnetization switching without an external magnetic field H_x at room temperature. (c) The SOT-induced magnetization switching with an external magnetic field H_x . The measurements were performed in Dev 3. (d) State-of-the-art of representative field-free SOT devices showing spin Hall conductivity $\sigma_{\text{SH}} = \theta_{\text{SH}} \sigma_c$ of related spin–orbit materials as a function of the power density $P = (J_{\text{sw}}^2 / \sigma_c)$ for the magnetization switching ($\text{WTe}_2/\text{Fe}_3\text{GeTe}_2$,²⁸ $\text{WTe}_2/\text{Fe}_3\text{GaTe}_2$,²⁹ $\text{TaIrTe}_4/\text{Ti}/\text{CoFeB}$,^{31,32} $\text{PtTe}_2/\text{WTe}_2/\text{CoFeB}$,³³).

the second harmonic signals at both $H = \pm 8.5$ T and the averaged result $V_{\text{avg}} = [V_{2\omega}(8.5 \text{ T}) - V_{2\omega}(-8.5 \text{ T})]/2$. This procedure rules out any other magnetoresistance signal present in the $\text{Fe}_5\text{GeTe}_2/\text{Pt}$ heterostructures. A detailed analysis of the data was presented in Note S2 and Figure S4. The averaged and fitting results at all fields are shown in Figure 4b. A further fitting of the extracted $V_{2\omega,A}$ vs $1/(H - H_k)$ and $V_{2\omega,P}$ vs $1/H$ are performed to obtain H_{DL} , V_{th} , and H_{FL} using eq 2 and eq 3, respectively (Figure 4c,d). The applied bias current dependence of the extracted parameters offers more precise results with a linear and parabolic fitting for $H_{\text{DL(FL)}}$ and V_{th} , respectively (Figure 4e). By using a parallel resistor model to estimate the current flowing through the Pt layer, we obtain $\Delta H_{\text{DL}}/J_{\text{ac}} = 0.06 \pm 0.01 \text{ mT per MA/cm}^2$ and $\Delta H_{\text{FL}}/J_{\text{ac}} = 8.64 \pm 0.51 \text{ mT per MA/cm}^2$. The thermal contribution to the harmonic signal $V_{\text{th}} \sim I^2$, suggests a vertical thermal gradient ∇T_z at $\text{Fe}_5\text{GeTe}_2/\text{Pt}/\text{SiO}_2/\text{Si}$, generating a $V_{\text{th}} \sim M_x \times \nabla T_z$.⁴⁴

Spin–Orbit Torque Magnetization Switching in $\text{Fe}_5\text{GeTe}_2/\text{Pt}$ Heterostructure at Room Temperature. Next, we investigate the magnetization switching of $\text{Fe}_5\text{GeTe}_2/\text{Pt}$ heterostructure at room temperature (as shown schematically in Figure 5a). As discussed earlier, the AHE signal with a clear remanence with an in-plane field sweep confirms a canted magnetization at room temperature. Similar to our low-temperature measurements, the SOT magnetization switching measurements of the $\text{Fe}_5\text{GeTe}_2/\text{Pt}$ bilayer structure show deterministic switching between two magnetic states by a pulse current induced in-plane damping-like torque, with a critical switching current density J_{sw} of $1.9 \times 10^7 \text{ A/cm}^2$ with no clear dependence on the direction of the external magnetic field (Figure 5b and Figure 5c). Such room temperature deterministic switching has also been observed in other devices (see Figure S5).

DISCUSSION

The canted magnetic anisotropy of Fe_5GeTe_2 is attributed to the $\sqrt{3} \times \sqrt{3}$ atomic crystal structure that exists due to Fe vacancies in Fe_5GeTe_2 ,^{38,47} agreeing well with our observations of the SOT experiments and magnetic properties in Fe_5GeTe_2 .⁴⁸ The in-plane external field (H_x) dependence measurements show that the sign of the SOT switching direction remains unchanged, confirming that the applied field does not play a major role in the symmetry breaking for the deterministic switching. Instead, the observation of field-free deterministic magnetization switching of $\text{Fe}_5\text{GeTe}_2/\text{Pt}$ heterostructure can be explained by considering the canted-perpendicular magnetization of Fe_5GeTe_2 .

To be noted, the calculation of SOT-induced switching efficiency η_{sw} based on the pulse-induced magnetization switching is usually overestimated.⁴⁹ The current-induced torques only need to overcome the depinning or nucleation barrier with the assistance of Joule heating, which is much smaller than the anisotropy barrier, so that the switching efficiency η_{sw} is usually much larger than the spin Hall angle θ_{SH} .⁴⁹ So, we calculate the spin Hall conductivity $\sigma_{\text{SH}} = \theta_{\text{SH}} \sigma_c$ (σ_c is the charge conductivity), which considers both spin–charge conversion efficiency θ_{SH} and the conductivity of the spin–orbit materials (SOMs) to minimize power consumption. This is a universal figure of merit to characterize the SOT performance.⁵⁰ Using the values obtained for our devices ($\theta_{\text{SH}} > 0.12$ and $\sigma_c = 2.5 \times 10^6 \text{ S/m}$, we estimate $\sigma_{\text{SH}} = (3.0 \sim 7.5) \times 10^5 \text{ } \text{h/2e } \Omega^{-1} \text{ m}^{-1}$, which is attributed to the transparent $\text{Fe}_5\text{GeTe}_2/\text{Pt}$ interface^{21,22} (see more details in Table S2)). Figure 5d shows the state-of-the-art of representative field-free SOT devices, showing spin Hall conductivity σ_{SH} of related spin–orbit materials as a function of the power density P of the representative field-free SOT devices. Our work on $\text{Fe}_5\text{GeTe}_2/\text{Pt}$ heterostructure is among the best field-free SOT devices in

terms of spin Hall conductivity σ_{SH} and the power consumption P . Furthermore, observing field-free and deterministic SOT magnetization switching of vdW magnets up to room temperature using conventional spin Hall materials such as Pt can have advantages over other systems.

CONCLUSIONS

In summary, we demonstrate an external magnetic field-free deterministic magnetization switching in $\text{Fe}_5\text{GeTe}_2/\text{Pt}$ heterostructures up to room temperature. The observation of such SOT-induced magnetization switching is enabled by the canted magnetization of Fe_5GeTe_2 . Detailed second harmonic Hall measurements and analysis show a large SOT-induced magnetization switching efficiency with spin Hall conductivity $\sigma_{\text{SH}} \sim 3 \times 10^5 \frac{\hbar}{2e} \Omega^{-1} \text{ m}^{-1}$. The SOT devices using $\text{Fe}_5\text{GeTe}_2/\text{Pt}$ heterostructures highlight the potential of using canted vdW magnetic material and conventional spin-orbit materials with large spin Hall conductivity. In the future, all-vdW heterostructures of Fe_5GeTe_2 can also be used together with topological materials having even larger charge-spin conversion properties. Encouragingly, the T_c of vdW magnetic materials can be further enhanced much beyond room temperature, and their magnetic properties can be engineered with alloys of Co^{51–53} and Ni.^{54,55} Combining spin-orbit materials with large charge-spin conversion efficiency and vdW magnets with faster magnetization dynamics can be envisioned as new building blocks for future energy-efficient spintronic applications.

METHODS/EXPERIMENTAL

Device Fabrication: The Pt layer (10 nm) is first globally deposited on a SiO_2/Si substrate with a Ti seed layer (2 nm). FGT flakes are exfoliated and transferred onto the Pt layer inside a Nitrogen gas glovebox. This is followed by patterning of the Pt and FGT films using electron beam lithography and Ar-ion plasma etching to define the Hall bar geometry.

Measurements: Transport measurements in Fe_5GeTe_2 and $\text{Fe}_5\text{GeTe}_2/\text{Pt}$ devices were performed in a vacuum cryostat with a magnetic field. The electronic measurements were carried out using the current source Keithley 6221 and nanometer 2182A. To monitor the longitudinal and Hall resistances, Keithley 2182A nanovoltmeters were used. For the current-induced switching measurements in the F₅GT/Pt devices, Keithley 2182A nanovoltmeters were used to monitor the response of the Hall resistances, whereas a Keithley 6221 AC source was used with a pulse current of 100 μs through the device. The harmonic measurement was performed using Lock in SR830 to measure in-phase first and out-of-phase second harmonic voltages with $f = 213.34 \text{ Hz}$, respectively. The second harmonic measurements in the high magnetic field range were carried out in the Quantum Design cryogen-free PPMS DynaCool system with an external electronic connection to Lock in SR830 to measure the first and second harmonic voltages.

XPS, ARPES, STM: XPS of the single crystal was probed at photon energy of 160 eV at 260 K. ARPES: The angle-resolved photoelectron spectroscopy (ARPES) measurements were performed at the MAX IV Laboratory Bloch beamline with high energy, angular, and spatial resolution (15 meV, < 0.15 degrees, 10 $\mu\text{m} \times 15 \mu\text{m}$). The measurements were done at 20 K at 138 eV photon energy. Single crystals of Fe_5GeTe_2 were cleaved in a high vacuum better than $8 \times 10^{-11} \text{ mbar}$. A deflector-type hemispherical analyzer from Scienta Omicron was used. STM: The scanning tunneling microscopy (STM) measurements were done at 300 K using the VT-XA model from Scienta Omicron.

ASSOCIATED CONTENT

Data Availability Statement

The data that support the findings of this study are available from the corresponding authors on reasonable request.

SI Supporting Information

The Supporting Information is available free of charge at <https://pubs.acs.org/doi/10.1021/acsnano.4c16826>.

Additional information and figures regarding the summary of the devices/samples and the corresponding measurement techniques; canted magnetic anisotropy of Fe_5GeTe_2 ; SOT efficiency of the $\text{Fe}_5\text{GeTe}_2/\text{Pt}$ heterostructure; SOT parameters of the measured $\text{Fe}_5\text{GeTe}_2/\text{Pt}$ devices ([PDF](#))

AUTHOR INFORMATION

Corresponding Authors

Bing Zhao – Department of Microtechnology and Nanoscience, Chalmers University of Technology, Göteborg SE-41296, Sweden; orcid.org/0000-0002-5560-6750; Email: zbing@chalmers.se

Saroj Prasad Dash – Department of Microtechnology and Nanoscience, Chalmers University of Technology, Göteborg SE-41296, Sweden; Wallenberg Initiative Materials Science for Sustainability, Department of Microtechnology and Nanoscience and Graphene Center, Chalmers University of Technology, Göteborg SE-41296, Sweden; orcid.org/0000-0001-7931-4843; Email: saroj.dash@chalmers.se

Authors

Lalit Pandey – Department of Microtechnology and Nanoscience, Chalmers University of Technology, Göteborg SE-41296, Sweden; Wallenberg Initiative Materials Science for Sustainability, Department of Microtechnology and Nanoscience, Chalmers University of Technology, Göteborg SE-41296, Sweden

Khadiza Ali – Department of Microtechnology and Nanoscience, Chalmers University of Technology, Göteborg SE-41296, Sweden; MAX IV Laboratory, Lund University, Lund SE-221 00, Sweden

Erdi Wang – Department of Microtechnology and Nanoscience, Chalmers University of Technology, Göteborg SE-41296, Sweden

Craig M. Polley – MAX IV Laboratory, Lund University, Lund SE-221 00, Sweden

Balasubramanian Thiagarajan – MAX IV Laboratory, Lund University, Lund SE-221 00, Sweden

Peter Makk – Department of Physics, Institute of Physics, Budapest University of Technology and Economics, Budapest H-1111, Hungary; MTA-BME Correlated van der Waals Structures Momentum Research Group, Budapest H-1111, Hungary; orcid.org/0000-0001-7637-4672

Marcos H. D. Guimarães – Zernike Institute for Advanced Materials, University of Groningen, Groningen 9747AG, the Netherlands; orcid.org/0000-0002-8150-4379

Complete contact information is available at:

<https://pubs.acs.org/10.1021/acsnano.4c16826>

Author Contributions

B.Z. and S.P.D. conceived the idea and designed the experiments. B.Z. and E.W. fabricated and characterized the devices with the support of L.P., K.A., C.M.P., and T.B. performed the XPS, ARPES, and STM measurements. B.Z.,

K.A., L.P., P.M., M.H.D.G., and S.P.D. analyzed and interpreted the experimental data, compiled the figures, and wrote the manuscript. S.P.D. supervised the research.

Notes

The authors declare no competing financial interest.

ACKNOWLEDGMENTS

The authors acknowledge financial support from the European Commission Graphene Flagship project 2DSPIN-TECH (No. 101135853), the 2D TECH VINNOVA competence center (No. 2019-00068), the FLAG-ERA project 2DSOTECH (VR No. 2021-05925), and MagicTune, as well as the Wallenberg Initiative Materials Science for Sustainability (WISE) funded by the Knut and Alice Wallenberg Foundation, the EU Graphene Flagship (Core 3, No. 881603), Swedish Research Council VR project grants (No. 2021-04821, No. 2018-07046), the Carl Tryggers Foundation, and the Graphene Center, AoA Nano, Materials, and Energy programs at Chalmers University of Technology. The authors acknowledge the help of staff at the Quantum Device Physics and Nanofabrication Laboratory in our department at Chalmers. Devices were fabricated at the Nanofabrication Laboratory, Myfab, MC2, Chalmers. The authors acknowledge MAX IV Laboratory for time on the Bloch Beamline, supported by the Swedish Research Council (No. 2018-07152), the Swedish Governmental Agency for Innovation Systems (No. 2018-04969), and Formas (No. 2019-02496), ERC Consolidator grant Twistrain. MHDG acknowledges the support from the European Research Council (ERC, 2D-OPTOSPIN, No. 101076932) and the Zernike Institute for Advanced Materials.

REFERENCES

- (1) Fert, A.; Ramesh, R.; Garcia, V.; Casanova, F.; Bibes, M. Electrical Control of Magnetism by Electric Field and Current-Induced Torques. *Rev. Mod. Phys.* **2024**, *96* (1), 015005.
- (2) Yakout, S. M. Spintronics: Future Technology for New Data Storage and Communication Devices. *J. Supercond. Nov. Magn.* **2020**, *33* (9), 2557–2580.
- (3) Bhatti, S.; Sbiaa, R.; Hirohata, A.; Ohno, H.; Fukami, S.; Piramanayagam, S. N. Spintronics Based Random Access Memory: A Review. *Mater. Today* **2017**, *20* (9), 530–548.
- (4) Shao, Q.; Li, P.; Liu, L.; Yang, H.; Fukami, S.; Razavi, A.; Wu, H.; Wang, K.; Freimuth, F.; Mokrousov, Y.; Stiles, M. D.; Emori, S.; Hoffmann, A.; Akerman, J.; Roy, K.; Wang, J.-P.; Yang, S.-H.; Garello, K.; Zhang, W. Roadmap of Spin–Orbit Torques. *IEEE Trans. Magn.* **2021**, *57* (7), 1–39.
- (5) Mihai Miron, I.; Gaudin, G.; Auffret, S.; Rodmacq, B.; Schuhl, A.; Pizzini, S.; Vogel, J.; Gambardella, P. Current-Driven Spin Torque Induced by the Rashba Effect in a Ferromagnetic Metal Layer. *Nat. Mater.* **2010**, *9* (3), 230–234.
- (6) Miron, I. M.; Garello, K.; Gaudin, G.; Zermatten, P. J.; Costache, M. V.; Auffret, S.; Bandiera, S.; Rodmacq, B.; Schuhl, A.; Gambardella, P. Perpendicular Switching of a Single Ferromagnetic Layer Induced by In-Plane Current Injection. *Nature* **2011**, *476* (7359), 189–193.
- (7) Lee, S. W.; Lee, K. J. Emerging Three-Terminal Magnetic Memory Devices. *Proc. IEEE* **2016**, *104* (10), 1831–1843.
- (8) Grollier, J.; Querlioz, D.; Camsari, K. Y.; Everschor-Sitte, K.; Fukami, S.; Stiles, M. D. Neuromorphic Spintronics. *Nat. Electron.* **2020**, *3* (7), 360–370.
- (9) Sengupta, A.; Choday, S. H.; Kim, Y.; Roy, K. Spin Orbit Torque Based Electronic Neuron. *Appl. Phys. Lett.* **2015**, *106* (14), 143701.
- (10) Manchon, A.; Železný, J.; Miron, I. M.; Jungwirth, T.; Sinova, J.; Thiaville, A.; Garello, K.; Gambardella, P. Current-Induced Spin Orbit Torques in Ferromagnetic and Antiferromagnetic Systems. *Rev. Mod. Phys.* **2019**, *91* (3), 035004.
- (11) Baek, S. H. C.; Amin, V. P.; Oh, Y. W.; Go, G.; Lee, S. J.; Lee, G. H.; Kim, K. J.; Stiles, M. D.; Park, B. G.; Lee, K. J. Spin Currents and Spin–Orbit Torques in Ferromagnetic Trilayers. *Nat. Mater.* **2018**, *17* (6), 509–513.
- (12) Kurebayashi, H.; Garcia, J. H.; Khan, S.; Sinova, J.; Roche, S. Symmetry and Spin Transport in van Der Waals Layered Systems. *Nat. Rev. Phys.* **2022**, *4* (3), 150–166.
- (13) Huang, B.; McGuire, M. A.; May, A. F.; Xiao, D.; Jarillo-Herrero, P.; Xu, X. Emergent Phenomena and Proximity Effects in Two-Dimensional Magnets and Heterostructures. *Nat. Mater.* **2020**, *19* (12), 1276–1289.
- (14) Mak, K. F.; Shan, J.; Ralph, D. C. Probing and Controlling Magnetic States in 2D Layered Magnetic Materials. *Nat. Rev. Phys.* **2019**, *1* (11), 646–661.
- (15) Gibertini, M.; Koperski, M.; Morpurgo, A. F.; Novoselov, K. S. Magnetic 2D Materials and Heterostructures. *Nat. Nanotechnol.* **2019**, *14* (5), 408–419.
- (16) Liu, L.; Lee, O. J.; Gudmundsen, T. J.; Ralph, D. C.; Buhrman, R. A. Current-Induced Switching of Perpendicularly Magnetized Magnetic Layers Using Spin Torque from the Spin Hall Effect. *Phys. Rev. Lett.* **2012**, *109* (9), 096602.
- (17) Liu, L.; Qin, Q.; Lin, W.; Li, C.; Xie, Q.; He, S.; Shu, X.; Zhou, C.; Lim, Z.; Yu, J.; Lu, W.; Li, M.; Yan, X.; Pennycook, S. J.; Chen, J. Current-Induced Magnetization Switching in All-Oxide Heterostructures. *Nat. Nanotechnol.* **2019**, *14* (10), 939–944.
- (18) Zheng, Z.; Zhang, Y.; Lopez-Dominguez, V.; Sánchez-Tejerina, L.; Shi, J.; Feng, X.; Chen, L.; Wang, Z.; Zhang, Z.; Zhang, K.; Hong, B.; Xu, Y.; Zhang, Y.; Carpentieri, M.; Fert, A.; Finocchio, G.; Zhao, W.; Amiri, P. K. Field-Free Spin-Orbit Torque-Induced Switching of Perpendicular Magnetization in a Ferrimagnetic Layer with a Vertical Composition Gradient. *Nat. Commun.* **2021**, *12* (1), 4555.
- (19) Liu, L.; Zhou, C.; Shu, X.; Li, C.; Zhao, T.; Lin, W.; Deng, J.; Xie, Q.; Chen, S.; Zhou, J.; Guo, R.; Wang, H.; Yu, J.; Shi, S.; Yang, P.; Pennycook, S.; Manchon, A.; Chen, J. Symmetry-Dependent Field-Free Switching of Perpendicular Magnetization. *Nat. Nanotechnol.* **2021**, *16* (3), 277–282.
- (20) Cui, B.; Wu, H.; Li, D.; Razavi, S. A.; Wu, D.; Wong, K. L.; Chang, M.; Gao, M.; Zuo, Y.; Xi, L.; Wang, K. L. Field-Free Spin–Orbit Torque Switching of Perpendicular Magnetization by the Rashba Interface. *ACS Appl. Mater. Interfaces* **2019**, *11* (42), 39369–39375.
- (21) Alghamdi, M.; Lohmann, M.; Li, J.; Jothi, P. R.; Shao, Q.; Aldosary, M.; Su, T.; Fokwa, B. P. T.; Shi, J. Highly Efficient Spin-Orbit Torque and Switching of Layered Ferromagnet Fe₃GeTe₂. *Nano Lett.* **2019**, *19* (7), 4400–4405.
- (22) Wang, X.; Tang, J.; Xia, X.; He, C.; Zhang, J.; Liu, Y.; Wan, C.; Fang, C.; Guo, C.; Yang, W.; Guang, Y.; Zhang, X.; Xu, H.; Wei, J.; Liao, M.; Lu, X.; Feng, J.; Li, X.; Peng, Y.; Wei, H.; Yang, R.; Shi, D.; Zhang, X.; Han, Z.; Zhang, Z.; Zhang, G.; Yu, G.; Han, X. Current-Driven Magnetization Switching in a van Der Waals Ferromagnet Fe₃GeTe₂. *Sci. Adv.* **2019**, *5* (8), No. eaaw8904.
- (23) Li, W.; Zhu, W.; Zhang, G.; Wu, H.; Zhu, S.; Li, R.; Zhang, E.; Zhang, X.; Deng, Y.; Zhang, J.; Zhao, L.; Chang, H.; Wang, K. Room-Temperature van Der Waals Ferromagnet Switching by Spin-Orbit Torques. *Adv. Mater.* **2023**, *35* (51), 2303688.
- (24) Kajale, S. N.; Nguyen, T.; Chao, C. A.; Bono, D. C.; Boonkird, A.; Li, M.; Sarkar, D. Current-Induced Switching of a van Der Waals Ferromagnet at Room Temperature. *Nat. Commun.* **2024**, *15* (1), 1485.
- (25) Mogi, M.; Yasuda, K.; Fujimura, R.; Yoshimi, R.; Ogawa, N.; Tsukazaki, A.; Kawamura, M.; Takahashi, K. S.; Kawasaki, M.; Tokura, Y. Current-Induced Switching of Proximity-Induced Ferromagnetic Surface States in a Topological Insulator. *Nat. Commun.* **2021**, *12* (1), 1404.
- (26) Choi, G. S.; Park, S.; An, E.-S.; Bae, J.; Shin, I.; Kang, B. T.; Won, C. J.; Cheong, S.; Lee, H.; Lee, G.; Cho, W.-J.; Kim, J. S. Highly Efficient Room-Temperature Spin-Orbit-Torque Switching in a Van

- Der Waals Heterostructure of Topological Insulator and Ferromagnet. *Adv. Sci.* **2024**, *11* (21), 2400893.
- (27) Guillet, T.; Galceran, R.; Sierra, J. F.; Belarre, F. J.; Ballesteros, B.; Costache, M. V.; Dosenovic, D.; Okuno, H.; Marty, A.; Jamet, M.; Bonell, F.; Valenzuela, S. O. Spin–Orbit Torques and Magnetization Switching in $(\text{Bi}, \text{Sb})_2\text{Te}_3/\text{Fe}_3$ GeTe₂ Heterostructures Grown by Molecular Beam Epitaxy. *Nano Lett.* **2024**, *24* (3), 822–828.
- (28) Kao, I.-H.; Muzzio, R.; Zhang, H.; Zhu, M.; Gobbo, J.; Yuan, S.; Weber, D.; Rao, R.; Li, J.; Edgar, J. H.; Goldberger, J. E.; Yan, J.; Mandrus, D. G.; Hwang, J.; Cheng, R.; Katoch, J.; Singh, S. Deterministic Switching of a Perpendicularly Polarized Magnet Using Unconventional Spin–Orbit Torques in WTe₂. *Nat. Mater.* **2022**, *21* (9), 1029–1034.
- (29) Kajale, S. N.; Nguyen, T.; Hung, N. T.; Li, M.; Sarkar, D. Field-free deterministic switching of all–van der Waals spin-orbit torque system above room temperature. *Sci. Adv.* **2024**, *10* (11), eadk8669.
- (30) Bainsla, L.; Zhao, B.; Behera, N.; Hoque, A. M.; Sjöström, L.; Martinelli, A.; Abdel-Hafiez, M.; Åkerman, J.; Dash, S. P. Large out-of-plane spin–orbit torque in topological Weyl semimetal TaIrTe₄. *Nat. Commun.* **2024**, *15* (1), 4649.
- (31) Liu, Y.; Shi, G.; Kumar, D.; Kim, T.; Shi, S.; Yang, D.; Zhang, J.; Zhang, C.; Wang, F.; Yang, S.; Pu, Y.; Yu, P.; Cai, K.; Yang, H. Field-Free Switching of Perpendicular Magnetization at Room Temperature Using out-of-Plane Spins from TaIrTe₄. *Nat. Electron.* **2023**, *6* (10), 732–738.
- (32) Zhang, Y.; Xu, H.; Jia, K.; Lan, G.; Huang, Z.; He, B.; He, C.; Shao, Q.; Wang, Y.; Zhao, M.; Ma, T.; Dong, J.; Guo, C.; Cheng, C.; Feng, J.; Wan, C.; Wei, H.; Shi, Y.; Zhang, G.; Han, X.; Yu, G. Room Temperature Field-Free Switching of Perpendicular Magnetization through Spin-Orbit Torque Originating from Low-Symmetry Type II Weyl Semimetal. *Sci. Adv.* **2023**, *9* (44), adg981.
- (33) Wang, F.; Shi, G.; Kim, K.-W.; Park, H.-J.; Jang, J. G.; Tan, H. R.; Lin, M.; Liu, Y.; Kim, T.; Yang, D.; Zhao, S.; Lee, K.; Yang, S.; Soumyanarayanan, A.; Lee, K.-J.; Yang, H. Field-Free Switching of Perpendicular Magnetization by Two-Dimensional PtTe₂/WTe₂ van Der Waals Heterostructures with High Spin Hall Conductivity. *Nat. Mater.* **2024**, *23* (6), 768–774.
- (34) Pandey, L.; Zhao, B.; Tenzin, K.; Ngalo, R.; Lamparská, V.; Bangar, H.; Ali, A.; Abdel-Hafiez, M.; Zhang, G.; Wu, H.; Chang, H.; Sjöström, L.; Rout, P.; Ślawińska, J.; Dash, S. P. Energy-efficient field-free unconventional spin-orbit torque magnetization switching dynamics in van der Waals heterostructures. *arXiv* **2024**, arXiv:2408.13095v2.
- (35) MacNeill, D.; Stiehl, G. M.; Guimaraes, M. H. D.; Buhrman, R. A.; Park, J.; Ralph, D. C. Control of Spin–Orbit Torques through Crystal Symmetry in WTe₂/Ferromagnet Bilayers. *Nat. Phys.* **2017**, *13* (3), 300–305.
- (36) Zhao, B.; Karpik, B.; Khokhriakov, D.; Johansson, A.; Hoque, A. M.; Xu, X.; Jiang, Y.; Mertig, I.; Dash, S. P. Unconventional Charge–Spin Conversion in Weyl-Semimetal WTe₂. *Adv. Mater.* **2020**, *32* (38), 2000818.
- (37) Gupta, V.; Cham, T. M.; Stiehl, G. M.; Bose, A.; Mittelstaedt, J. A.; Kang, K.; Jiang, S.; Mak, K. F.; Shan, J.; Buhrman, R. A.; Ralph, D. C. Manipulation of the van Der Waals Magnet Cr₂Ge₂Te₆by Spin-Orbit Torques. *Nano Lett.* **2020**, *20* (10), 7482–7488.
- (38) Zhao, B.; Ngalo, R.; Ghosh, S.; Ershadrad, S.; Gupta, R.; Ali, K.; Hoque, A. M.; Karpik, B.; Khokhriakov, D.; Polley, C.; Thiagarajan, B.; Kalaboukhov, A.; Svedlindh, P.; Sanyal, B.; Dash, S. P. A Room-Temperature Spin-Valve with van Der Waals Ferromagnet Fe₅GeTe₂/Graphene Heterostructure. *Adv. Mater.* **2023**, *35* (16), 2209113.
- (39) May, A. F.; Ovchinnikov, D.; Zheng, Q.; Hermann, R.; Calder, S.; Huang, B.; Fei, Z.; Liu, Y.; Xu, X.; McGuire, M. A. Ferromagnetism Near Room Temperature in the Cleavable van Der Waals Crystal Fe₅FeTe₂. *ACS Nano* **2019**, *13* (4), 4436–4442.
- (40) Alahmed, L.; Nepal, B.; Macy, J.; Zheng, W.; Casas, B.; Sapkota, A.; Jones, N.; Mazza, A. R.; Brahlek, M.; Jin, W.; Mahjouri-Samani, M.; Zhang, S. S. L.; Mewes, C.; Balicas, L.; Mewes, T.; Li, P. Magnetism and Spin Dynamics in Room-Temperature van Der Waals Magnet Fe₅GeTe₂. *2D Mater.* **2021**, *8* (4), 045030.
- (41) Zhang, H.; Chen, R.; Zhai, K.; Chen, X.; Caretta, L.; Huang, X.; Chopdekar, R. V.; Cao, J.; Sun, J.; Yao, J.; Birgeneau, R.; Ramesh, R. Itinerant Ferromagnetism in van Der Waals Fe₅–xGeTe₂ Crystals above Room Temperature. *Phys. Rev. B* **2020**, *102* (6), 064417.
- (42) Zhang, S.; Levy, P. M.; Fert, A. Mechanisms of Spin-Polarized Current-Driven Magnetization Switching. *Phys. Rev. Lett.* **2002**, *88* (23), 236601.
- (43) Shapiro, A.; Levy, P. M.; Zhang, S. Self-Consistent Treatment of Nonequilibrium Spin Torques in Magnetic Multilayers. *Phys. Rev. B* **2003**, *67* (10), 104430.
- (44) Avci, C. O.; Garello, K.; Gabureac, M.; Ghosh, A.; Fuhrer, A.; Alvarado, S. F.; Gambardella, P. Interplay of Spin-Orbit Torque and Thermoelectric Effects in Ferromagnet/Normal-Metal Bilayers. *Phys. Rev. B* **2014**, *90* (22), 224427.
- (45) Takeuchi, Y.; Zhang, C.; Okada, A.; Sato, H.; Fukami, S.; Ohno, H. Spin-Orbit Torques in High-Resistivity-W/CoFeB/MgO. *Appl. Phys. Lett.* **2018**, *112* (19), 192408.
- (46) Lau, Y.-C.; Hayashi, M. Spin Torque Efficiency of Ta, W, and Pt in Metallic Bilayers Evaluated by Harmonic Hall and Spin Hall Magnetoresistance Measurements. *Jpn. J. Appl. Phys.* **2017**, *56* (8), 0802B5.
- (47) Ly, T. T.; Park, J.; Kim, K.; Ahn, H.-B.; Lee, N. J.; Kim, K.; Park, T.-E.; Duvjur, G.; Lam, N. H.; Jang, K.; You, C.-Y.; Jo, Y.; Kim, S. K.; Lee, C.; Kim, S.; Kim, J. Direct Observation of Fe-Ge Ordering in Fe₅–xGeTe₂ Crystals and Resultant Helimagnetism. *Adv. Funct. Mater.* **2021**, *31* (17), 2009758.
- (48) Li, Z.; Xia, W.; Su, H.; Yu, Z.; Fu, Y.; Chen, L.; Wang, X.; Yu, N.; Zou, Z.; Guo, Y. Magnetic Critical Behavior of the van Der Waals Fe₅GeTe₂ Crystal with near Room Temperature Ferromagnetism. *Sci. Rep.* **2020**, *10* (1), 15345.
- (49) Zhu, L.; Ralph, D. C.; Buhrman, R. A. Maximizing Spin-Orbit Torque Generated by the Spin Hall Effect of Pt. *Appl. Phys. Rev.* **2021**, *8* (3), 031308.
- (50) Nguyen, M.-H.; Ralph, D. C.; Buhrman, R. A. Spin Torque Study of the Spin Hall Conductivity and Spin Diffusion Length in Platinum Thin Films with Varying Resistivity. *Phys. Rev. Lett.* **2016**, *116* (12), 126601.
- (51) Zhang, H.; Shao, Y.-T.; Chen, R.; Chen, X.; Susarla, S.; Raftrey, D.; Reichanadter, J. T.; Caretta, L.; Huang, X.; Settimeri, N. S.; Chen, Z.; Zhou, J.; Bourret-Courchesne, E.; Ercius, P.; Yao, J.; Fischer, P.; Neaton, J. B.; Muller, D. A.; Birgeneau, R. J.; Ramesh, R. A Room Temperature Polar Magnetic Metal. *Phys. Rev. Mater.* **2022**, *6* (4), 044403.
- (52) Tian, C.; Pan, F.; Xu, S.; Ai, K.; Xia, T.; Cheng, P. Tunable Magnetic Properties in van Der Waals Crystals (Fe₁–xCox)SGeTe₂. *Appl. Phys. Lett.* **2020**, *116* (20), 202402.
- (53) May, A. F.; Du, M.-H.; Cooper, V. R.; McGuire, M. A. Tuning Magnetic Order in the van Der Waals Metal Fe₅GeTe₂ by Cobalt Substitution. *Phys. Rev. Mater.* **2020**, *4* (7), 074008.
- (54) Hu, X.; Yao, D.-X.; Cao, K. (Fe₁–xNi_x)₅GeTe₂: An Antiferromagnetic Triangular Ising Lattice with Itinerant Magnetism. *Phys. Rev. B* **2022**, *106* (22), 224423.
- (55) Chen, X.; Shao, Y.-T.; Chen, R.; Susarla, S.; Hogan, T.; He, Y.; Zhang, H.; Wang, S.; Yao, J.; Ercius, P.; Muller, D. A.; Ramesh, R.; Birgeneau, R. J. Pervasive beyond Room-Temperature Ferromagnetism in a Doped van Der Waals Magnet. *Phys. Rev. Lett.* **2022**, *128* (21), 217203.